

Laminar burning characteristics of ethyl propionate, ethyl butyrate, ethyl acetate, gasoline and ethanol fuels

Badawy, Tawfik; Williamson, Jake; Xu, Hongming

DOI:

[10.1016/j.fuel.2016.06.087](https://doi.org/10.1016/j.fuel.2016.06.087)

License:

Creative Commons: Attribution-NonCommercial-NoDerivs (CC BY-NC-ND)

Document Version

Peer reviewed version

Citation for published version (Harvard):

Badawy, T, Williamson, J & Xu, H 2016, 'Laminar burning characteristics of ethyl propionate, ethyl butyrate, ethyl acetate, gasoline and ethanol fuels', *Fuel*, vol. 183, pp. 627-640. <https://doi.org/10.1016/j.fuel.2016.06.087>

[Link to publication on Research at Birmingham portal](#)

General rights

Unless a licence is specified above, all rights (including copyright and moral rights) in this document are retained by the authors and/or the copyright holders. The express permission of the copyright holder must be obtained for any use of this material other than for purposes permitted by law.

- Users may freely distribute the URL that is used to identify this publication.
- Users may download and/or print one copy of the publication from the University of Birmingham research portal for the purpose of private study or non-commercial research.
- User may use extracts from the document in line with the concept of 'fair dealing' under the Copyright, Designs and Patents Act 1988 (?)
- Users may not further distribute the material nor use it for the purposes of commercial gain.

Where a licence is displayed above, please note the terms and conditions of the licence govern your use of this document.

When citing, please reference the published version.

Take down policy

While the University of Birmingham exercises care and attention in making items available there are rare occasions when an item has been uploaded in error or has been deemed to be commercially or otherwise sensitive.

If you believe that this is the case for this document, please contact UBIRA@lists.bham.ac.uk providing details and we will remove access to the work immediately and investigate.

Laminar Burning Characteristics of Ethyl Propionate, Ethyl Butyrate, Ethyl Acetate, Gasoline and Ethanol Fuels

Tawfik Badawy^a, Jake Williamson^a, Hongming Xu^{a,b*}

^aUniversity of Birmingham, Birmingham, UK

^bState Key Laboratory of Automotive Safety and Energy, Tsinghua University, Beijing, China

Abstract

Ethyl esters have been considered as promising second-generation biofuel candidates, due to the available production from low grade biomass waste. Furthermore, with desirable energy densities, emissions performance, low solubility and higher Research Octane Number (RON), ethyl esters have proven attractive as fuel additives or alternatives for gasoline. In this study, high-speed schlieren photography was used to investigate the laminar burning characteristics of three ethyl ester fuels: ethyl acetate, ethyl propionate, and ethyl butyrate, in comparison with gasoline and ethanol at different initial temperatures and a variety of equivalence ratios, with an initial pressure of 0.1 MPa in a constant-volume vessel. For the five fuels, the stretched flame speeds, the un-stretched flame speeds, Markstein lengths, Markstein number, laminar burning velocities and laminar burning flux were calculated and analysed using the outwardly spherical flame method. The results show that for all examined initial temperatures (60°C, 90°C and 120°C) and equivalence ratios; ethanol had the highest un-stretched flame propagation speeds, whilst ethyl acetate (EA) had the lowest. At high initial temperatures (120°C), it was observed that the un-stretched flame speed trends of ethyl propionate (EP) and ethyl butyrate (EB) proved faster compared to gasoline, especially for rich conditions. The EB and EA flames demonstrated greater stability when compared to ethanol, EP, and gasoline. Analysis showed that ethanol yielded the fastest flame velocities, whilst EA consistently had the lowest among all the five fuels. The laminar burning velocities of the EP fuel were faster compared to EB and EA, whilst slower than ethanol and gasoline at 60°C. Further increase of the initial temperature, up to 120°C, showed the laminar flame speed of EP and EB to be faster than gasoline, indicating a fast-burning property, and potential of improving engine thermal efficiency.

Keywords: Ethyl acetate, ethyl propionate, ethyl butyrate, laminar burning velocity, schlieren optical method

*Corresponding author at: University of Birmingham, Birmingham, UK. Tel.: +441214144153.

E-mail address: h.m.xu@bham.ac.uk (H. M. Xu).

33 1. Introduction

34

35 With an ever present demand for energy worldwide combined with a growing population and reliance on
36 fuel powered applications (expected to grow by 57% until 2030) [1], the dependency on the finite and
37 diminishing supply of fossil derived fuels alongside the requirement for enhanced environmental consciousness
38 had resulted in vast investment, interest and continuous investigation into the future generation of alternative
39 fuels [2]. The prevalent interest in recent years considered the derivation, functionality and potential of
40 biological fuels, i.e. biofuels, sourced from biomass, with only 3% currently being economically exploited [2].
41 As such, research efforts have been focussed towards achieving performance characteristics of equal measure to
42 the current market (ethanol, gasoline and isooctane).

43

44 Bio-ethanol has been established as the prominent alternative to gasoline, being mass produced via alcohol
45 fermentation, cementing its matured status (relative to other alternatives) within the bioenergy market [3, 4].
46 However, whilst bio-ethanol afforded a high volume of production, it resulted in a large energy consumption
47 during processing, negating the benefits of its use as a primary fuel or component blend additive [1, 5]. This was
48 supported by unfavourable physical attributes, including: a low energy density (high gravimetric oxygen
49 content), high volatility, and high solubility (fuel quality affected by atmospheric water content, affecting its
50 long term stability) [6].

51

52 More recently, breakthroughs in mass production technologies broadened the spectrum of alternative fuels
53 sourced from biomass, with research into the flame and spray characteristics of fructose derived 2-methylfuran
54 (MF) and 2,5-dimethylfuran (DMF) yielding favourable results, with the fuels also exhibiting desirable
55 properties such as: high energy density (close to gasoline and between 30–40% greater than ethanol),
56 insolubility (high stability), high boiling point (less volatile), high research octane number (RON) (increased
57 efficiency and resistance to auto-ignition), and low energy consumption during production [5-8]. Furthermore,
58 investigations into second generation ester biofuels showed a reduction in production complexity, thereby
59 improving the efficiency of the necessary conversion steps (dictated by the engine specific fuel characteristics),
60 yielding high grade fuels without detriment to the net energy balance [9-12].

61

62 Due to the lower production cost for esters in the dual fermentation bio-refinery (DFB) process, a series of
63 ester oxygenates was evaluated recently for use as gasoline octane providers. It was found that EP, EB and EA
64 as gasoline additives provided a significant increase in the mean octane rating without a drastic change in vapor
65 pressure [13]. Ethyl ester fuels had several advantages over ethanol and ethers. First, they were not toxic.
66 Second, they had pleasant odor. Third, lower exhaust emissions of carbon monoxide, aldehydes and ketones
67 were expected because of the higher oxidation state of the esters [14]. Jenkins et al. [10] concluded that the ester
68 fuels were completely miscible with gasoline, enabling 50:50 blends, i.e. fuel integration instead of replacement,
69 with EA best suited to SI applications (low melting and flash point).

70
71 As an extension of the ester fuels application in spark ignition/compression ignition (SI/CI), research into
72 Homogeneous Charge Compression Ignition (HCCI) was conducted by Contino et al. [11-12] which concluded
73 that EA, EP and EB had a slower ignition rate than ethanol (agreed by Jenkins et al.) [10]. Furthermore, it was
74 shown that the esters offered no loss of power (energy content of stoichiometric mixtures were similar to
75 ethanol), with an improved mixture preparation (greater enthalpies of vaporisation), and good overall stability at
76 various equivalence ratios. Contino et al. [9] also investigated the engine performance and emissions of methyl
77 and ethyl valerates in SIE and found that the esters had a higher flame speed compared to Primary Reference
78 Fuels (PRF95). Moreover, no significant difference was observed for emissions and performance when the
79 engine was running with pure esters compared to PRF95.

80
81 **Table.1.** shows the general properties of the proposed fuels for baseline evaluation with ethanol and gasoline.
82 It was noticed that the three fuels demonstrated a reduction in LHV relative to gasoline (20–30% less, due to
83 their oxygen content which itself offered reduced soot formation), but an increase compared with ethanol (10–
84 20% for EP and EB). Furthermore, EP and EB exhibited similar boiling properties (98.89–120°C) and solubility
85 (low) to that of gasoline, benefitting from reduced volatility and high stability, whereas EA demonstrated
86 properties akin to ethanol, displaying an elevated RON (116) to accommodate higher compression ratios and
87 cycle efficiencies. Collectively, the fuels displayed latent heat of vaporisation similar to gasoline, with flash
88 points indicating potential diversity in application: EA (-2.78°C) in SI; EP and EB (12.22–18.89°C) in HCCI,
89 thereby cementing their combustion credentials [10].

90 The present paper aims to analyse and evaluate the laminar flame speed of three ester biofuels, namely: ethyl
91 acetate (EA), ethyl propionate (EP), and ethyl butyrate (EB), against gasoline and ethanol. Laminar flame

92 propagation characteristics are important fundamental physicochemical properties of a fuel–air mixture for
 93 validating the chemical reaction mechanisms and gaining a better understanding of the combustion process in
 94 engines [15, 16]. This study forms part of a series of experiments to explore the use of ethyl esters as additive or
 95 surrogate fuel for gasoline in SIE, utilising schlieren photography to investigate the laminar flame speed,
 96 Markstein length, Markstein number, laminar burning velocity and burning flux at different initial temperatures.

97

98 **Table.1.** General Properties of the research fuels (EA, EP, EB, ethanol and gasoline)

	Ethyl Acetate (EA)	Ethyl Propionate (EP)	Ethyl Butyrate (EB)	Ethanol	Gasoline
Linear structure formula	$\text{CH}_3\text{COOC}_2\text{H}_5$	$\text{CH}_3\text{CH}_2\text{COOC}_2\text{H}_5$	$\text{CH}_3\text{CH}_2\text{CH}_2\text{C}(\text{O})\text{OC}_2\text{H}_5$	CH_3OCH_3	Variable
Molecular formula	$\text{C}_4\text{H}_8\text{O}_2$	$\text{C}_5\text{H}_{10}\text{O}_2$	$\text{C}_6\text{H}_{12}\text{O}_2$	$\text{C}_2\text{H}_6\text{O}$	C_2 to C_{14}
H/C ratio	2.00	2.00	2.00	3.00	1.95
O/C ratio	0.50	0.40	0.33	0.50	0.02
Molecule schematic					Variable
Molecular mass (kg/kmol)	88.10	102.00	116.00	46.07	100–105
Gravimetric oxygen content (%)	36.36	31.37	27.59	34.78	2.35
Density @ 20 C (kg/m ³)	897	891	886	794.00	744.60
Water solubility	High	Low	Low	High (>100mg/ml @73°F)	Insoluble
Boiling point (°C)	77.22	98.89	120.00	77.30	96.30
Flash point (°C)	-2.78	12.22	18.89	17.22	-42.7
Research octane number (RON)	116.00	–	–	110.00	96.80
Stoichiometric air-fuel ratio	7.80	8.74	9.46	8.25	14.13
LHV (MJ/kg)	23.79	26.53	28.64	26.90	42.90
LHV (MJ/L)	21.34	23.64	25.38	21.36	31.90

99

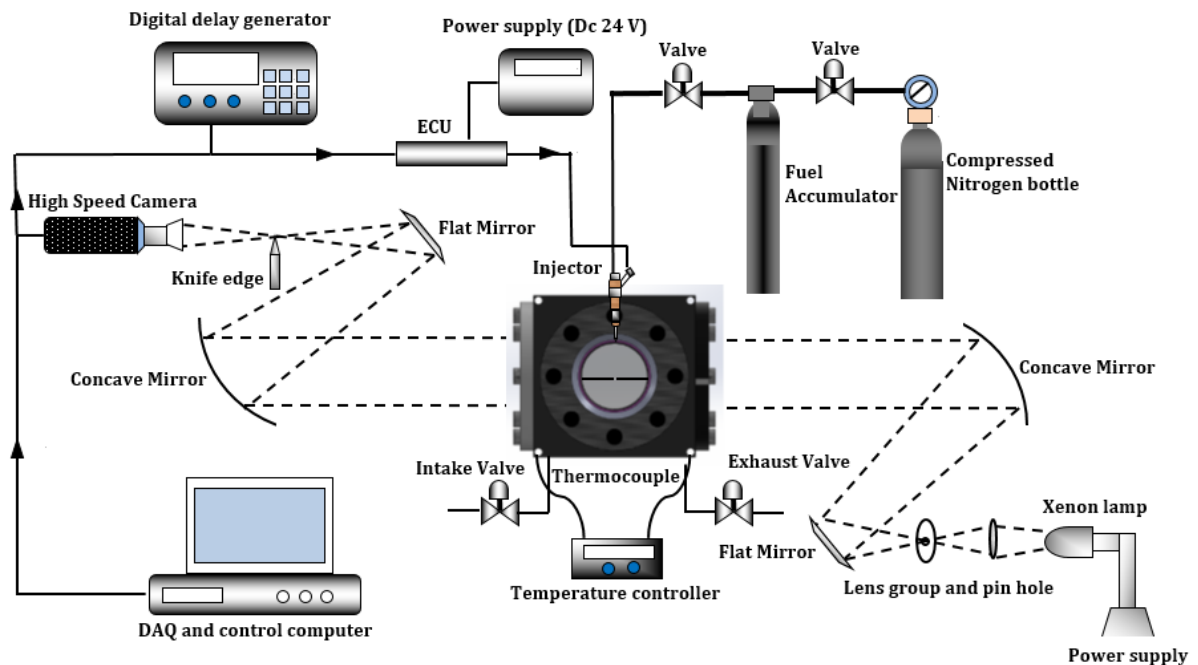
100 **2. Experimental setup**

101 **2.1 Schlieren optical method**

102

103 The laboratory setup for experimentation was a replication of the approach as detailed by Tian et al. [5] and
 104 Ma et al. [7] with Figure.1 providing a detailed schematic of the arrangement. As shown, a constant volume
 105 combustion vessel with two circular quartz observation windows (100 mm diameter) was utilised, alongside
 106 eight heating elements, installed at each corner. Temperature modulation of the vessel was implemented via
 107 closed loop control, to monitor the heating elements described and allow continuous observation of the fuel-air
 108 mixture condition within the chamber. The fuel injection strategy was fulfilled through a gasoline direct

109 injection (GDI) nozzle, which was mounted in the top cover of the vessel, and was driven by an ECU-computer
110 system. Finally, to achieve the necessary spark for ignition, a pair of tungsten electrodes was positioned in the
111 centre of the vessel, with a pressure release valve featured for safety purposes, operating at 0.7 MPa.



112

113

Figure.1. Schematic diagram for schlieren set up

114 To begin experimentation, a point light source was generated, utilising a 500 W xenon lamp combined with
115 a lens array, prior to an adjustable aperture. This light source was directed at a concave mirror to yield a parallel
116 beam, which passed through the vessel chamber via the aforementioned observation windows, illuminating the
117 test environment. Following this, the parallel beam was then collected at a second concave mirror on the
118 opposite side of the vessel, which integrated the light prior to its intersection by a knife edge, to achieve the
119 desired schlieren effect (two dimensional imaging). To document the combustion events, a Phantom research
120 V710 high-speed camera was utilised (synchronised with spark timing; no recorded delay), with a capture rate
121 of 10 kHz (10,000 frames per second) and resolution of 800 x 800 pixels.

122

123 Compressed air was used to scavenge the burned gases in the exhaust. After flushing and before each test,
124 the vessel chamber was opened to the ambient air until the air temperature inside the vessel stabilized at the test
125 point. Once the temperature stabilized, the valves to the chamber were closed and the fuel was injected to form a
126 homogenous fuel-air mixture, remaining undisturbed for a minimum of five minutes to guarantee homogeneity
127 and a relative state of inactivity. Following this, the mixture was ignited via electrode spark, which

128 simultaneously switched the camera on to record. After the combustion event, the burned products were
129 extracted from the vessel chamber, enabling the experiment to be restarted. To ensure confidence in procedure,
130 each test was repeated a minimum of three times, with the process being pursued at initial temperatures of 60°C,
131 90°C and 120°C and a variety of ϕ from 0.8 to 1.4.

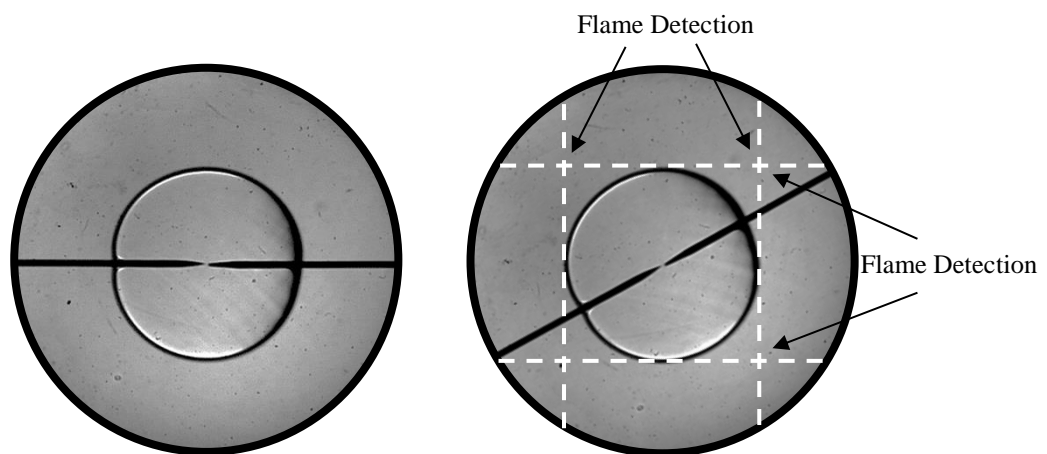
132

133 3. Image processing

134

135 Following experimentation, the captured schlieren images were analysed via an in-house MATLAB program,
136 to evaluate the basic laminar flame characteristics. To eliminate the negative influence of factors including spark
137 ignition and flame quenching during such analysis, the flame radii were measured in four directions at an
138 inclined angle of 45° relative to the electrodes (see Figure. 2). The captured images were 8-bit grayscale images.
139 The images were processed using the following steps. Firstly, the raw flame images were background corrected
140 using a frame prior to the start of the flame. This step eliminated any background noise. Then, a threshold of 5%
141 was used to convert the background corrected image to a binary image. Finally, the boundary of the flame area
142 can be detected based on the binary image. Observation of the flame radius was isolated to the vertical and
143 horizontal directions, in the range of 6–25 mm, as deemed sufficient by previous studies [5, 7]. All results in the
144 analysis were then averaged from the three tests, as discussed.

145



146 **Figure.2.** Laminar flame radius detection (left: original image; right: 45° rotated image)

147

148 To evaluate the laminar burning velocities, various parameters required definition, with the first being the
149 instantaneous rate of change of the flame radius (r_u), namely the stretched laminar flame speed (S_n):

$$S_n = \frac{dr_u}{dt} \quad (1)$$

150 where t was the time after ignition. By knowing the stretched laminar flame speed, the stretch rate (α) was
 151 calculated by [17, 18]:

$$\alpha = \frac{2S_n}{r_u} \quad (2)$$

152 The linear correlations between the stretch rate and flame speed were expressed by [17, 18]:
 153

$$S_n = S_s - L_b \times \alpha \quad (3)$$

154 where S_s represented the un-stretched flame speed flame speed, and L_b expressed the Markstein length.
 155 Determination of S_s was achieved by extrapolating S_n to a zero stretch rate, whilst L_b was the negative value of
 156 the gradient of the flame propagation speed against the stretch rate curve.

157 The laminar burning velocity (u_1) could be obtained from the equation [17, 18]:
 158

$$u_1 = S_s \times \frac{\rho_b}{\rho_u} \quad (4)$$

159 where ρ_b and ρ_u were the burned and unburned mixture densities, respectively. Assuming the pressure was
 160 constant, the burned (ρ_b) and unburned gas densities (ρ_u) could be found from the conservation of mass equation:

$$\frac{\rho_b}{\rho_u} = \frac{V_u}{V_b} = \frac{n_u T_u}{n_b T_b} \quad (5)$$

161 where n_u and n_b were the number of moles of reactants and products, and T_u and T_b were the initial and adiabatic
 162 flame temperatures.

163 The adiabatic flame temperatures were calculated using HPFLAME [19], which incorporates the Olikara and
 164 Borman equilibrium routines [20].

165 The flame thickness was calculated by the ratio of kinematic viscosity to laminar flame velocity via [21, 22]:

$$\delta_L = \frac{\nu}{u_1} \quad (6)$$

166 The Markstein number was calculated from the ratio of Markstein length to the flame thickness [17]:
 167

$$M_a = \frac{L_b}{\delta_L} \quad (7)$$

168 The laminar burning flux, which reveals the eigenvalue of the flame propagation, was calculated by [17]:
 169

$$f = u_1 \times \rho_u \quad (8)$$

170

171 4. Results and discussion

172 4.1. System validation

173

174

175

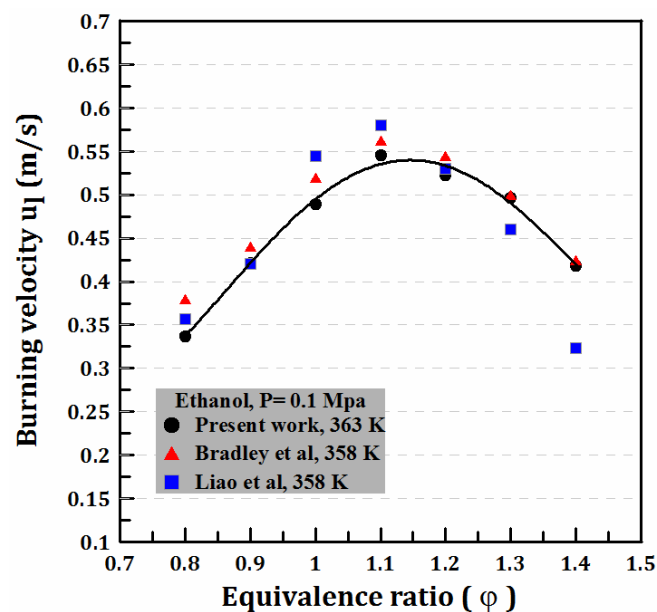
176

177

178

179

In order to validate the system setup and procedures used, laminar burning velocities of ethanol-air mixtures at 0.1MPa initial pressure and 363 K initial temperature were calculated and compared with available data from published literature. Figure.3 indicates that the current measurement proved consistent with available data, and demonstrated good agreement with the widely accepted result of Bradley et al. [23], and in addition, Liao et al. [24]. This validates the present experimental setup and methodology.



180

181 Figure.3. Laminar burning velocity of ethanol at 0.1 MPa and 363K in this work, compared with [23, 24]

182 4.2. Flame morphology

183

184 Figure.4 demonstrates the time elapsed flame propagation of the five fuels at stoichiometric conditions with

185 an initial temperature of 90°C and an initial pressure of 0.1 MPa. As shown, ethanol exhibited the greatest flame

186 propagation speeds among the five fuels, whilst EA displayed the lowest. EP proved slower than ethanol, but

187 faster than gasoline. EB was almost comparable with gasoline. As the flames approached the vessel wall, the

188 spherical profiles became distorted, with a flatter surface on the upper side due to the influence of the internal

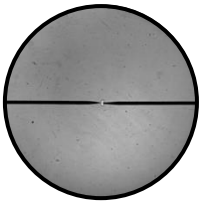
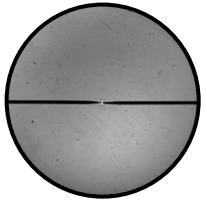
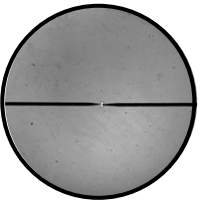
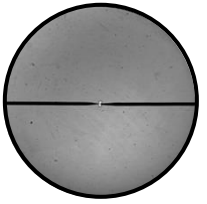
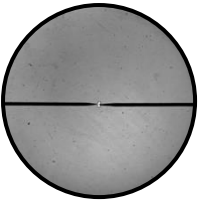
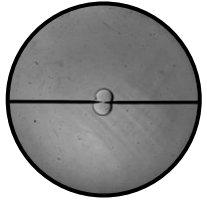
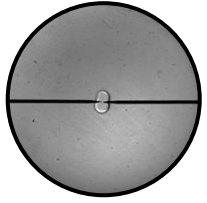
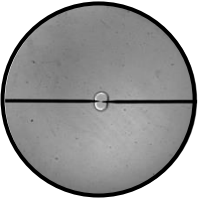
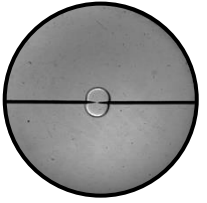
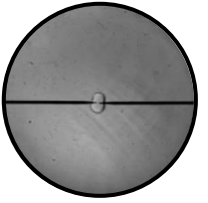
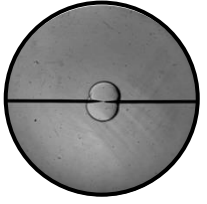
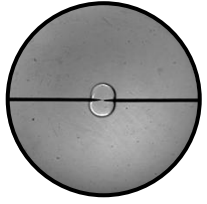
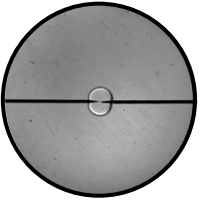
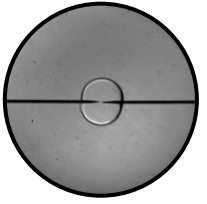
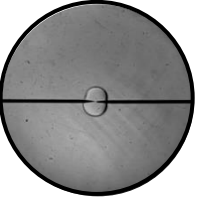
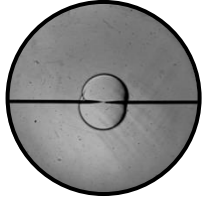
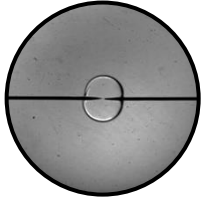
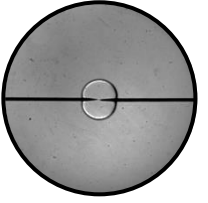
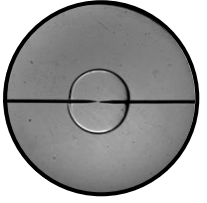
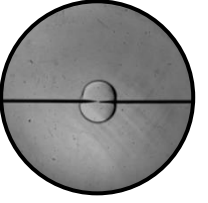
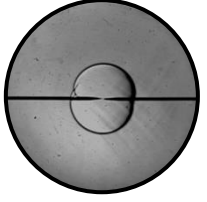
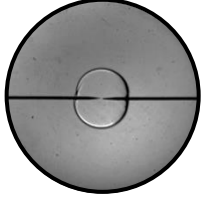
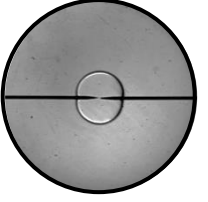
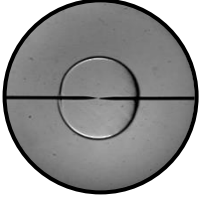
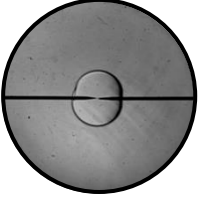
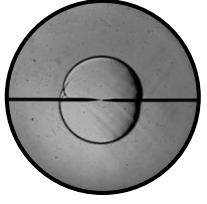
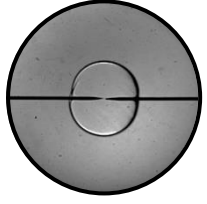
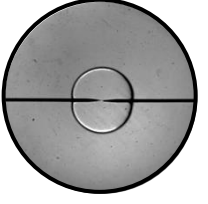
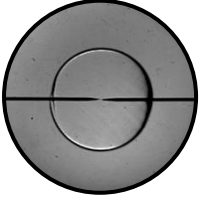
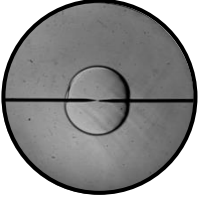
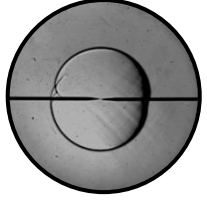
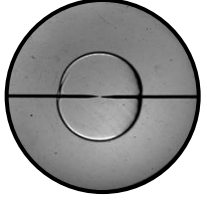
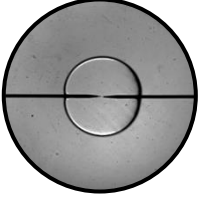
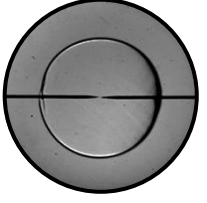
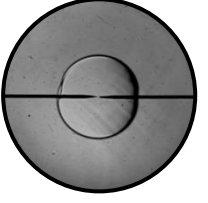
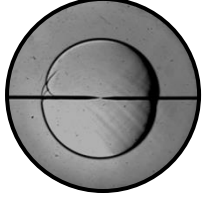
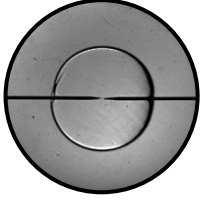
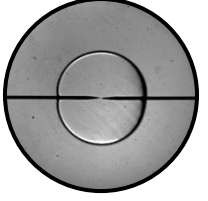
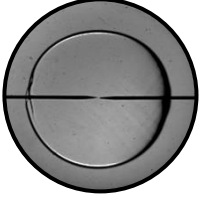
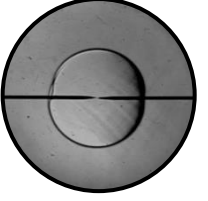
189 vessel geometry [25]. Due to the quenching effect of the electrodes, all flame propagation speeds were slower

190 along the direction of the electrodes than in the vertical direction, thus the flame was not perfectly spherical. The

191 wrinkling near the electrodes was attributed to the quenching effect. All images used for calculation were

192 chosen such that significant wrinkling on the flame front surface (which may affect the results), was avoided.

193

Time elapsed	EP	EB	EA	Ethanol	Gasoline
1 ms					
2.5 ms					
4 ms					
5.5 ms					
7 ms					
8.5 ms					
10 ms					
11.5 ms					

194

195 **Figure.4.** Flame images of stoichiometric fuel-air mixtures at initial temperature of 90°C and ambient pressure

4.3.1. Stretched flame propagation speed

The stretched flame propagation speed versus stretch rate (marked as α , in the figures) for the five fuels at different equivalence ratios under 120°C are given in Figure.5. During the early stages of flame propagation (when the flame radius was small), the stretch rate of flame front surface was large and the flame propagation speed proved low. As the flame propagated outwardly, the flame stretch rate decreased and the flame propagation speed increased. Removal of data affected by ignition energy and the electrodes during the early stage of flame development yielded a linear correlation for the stretched flame speed and the flame stretch rate as shown in Figure.5. The linear correlation between the flame stretch rate and the flame radius at a large stretch rate was considered representative of the laminar flame characteristics [5]. However, in some cases, non-linearity appeared at large stretch rates. For instance, at $\phi=1$ for gasoline and EP, the results showed a bending trend at maximum stretch rates. In order to evaluate the un-stretched flame speed and Markstein length correctly, those points deemed too far from linearity were removed as poor data. This was enforced by a deviation constraint of less than 5% required for the fitting result, with the offset to the fitting line of the individual points also restricted to within 5%, whilst retaining as many data points as practicably possible.

Recently, the nonlinear correlation is used to process the data, especially for the lean and rich mixtures. Li et al. [26] demonstrated the comparison of laminar flame speeds with linear and nonlinear methodologies for n-Pentanol-air mixtures at various initial conditions. They revealed that the results yielded in the two methods were closely matched at all conditions with a slight difference for lean and rich mixtures. However, the differences between the two groups of data were smaller than $2 \text{ cm}\cdot\text{s}^{-1}$, within the uncertainty of measurements. Therefore, for this study the linear methodology is used for the laminar flame speeds calculations.

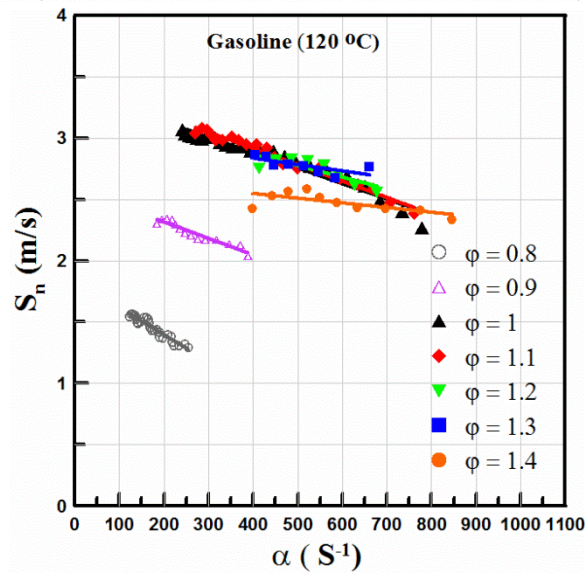
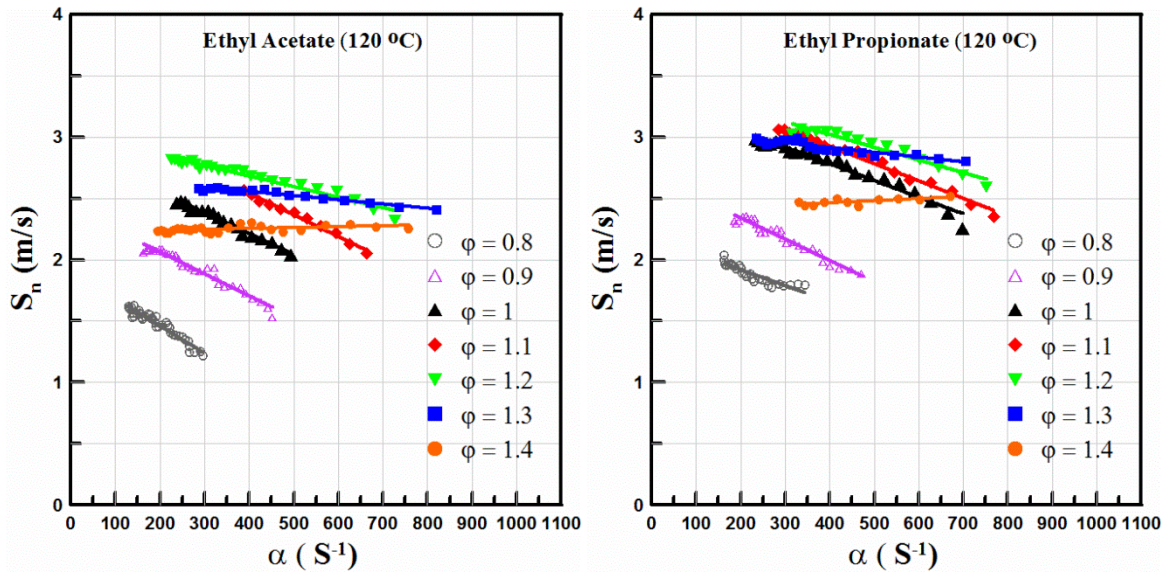
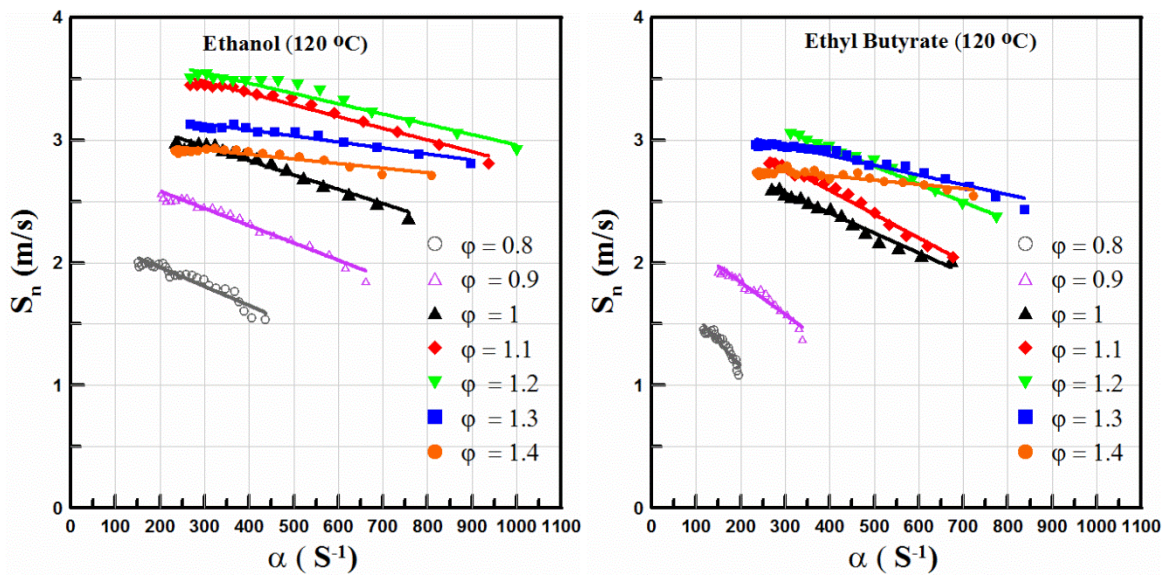


Figure 5: Stretched flame speed of the test fuels at 120°C initial temperature at different equivalence ratios and stretch rates.

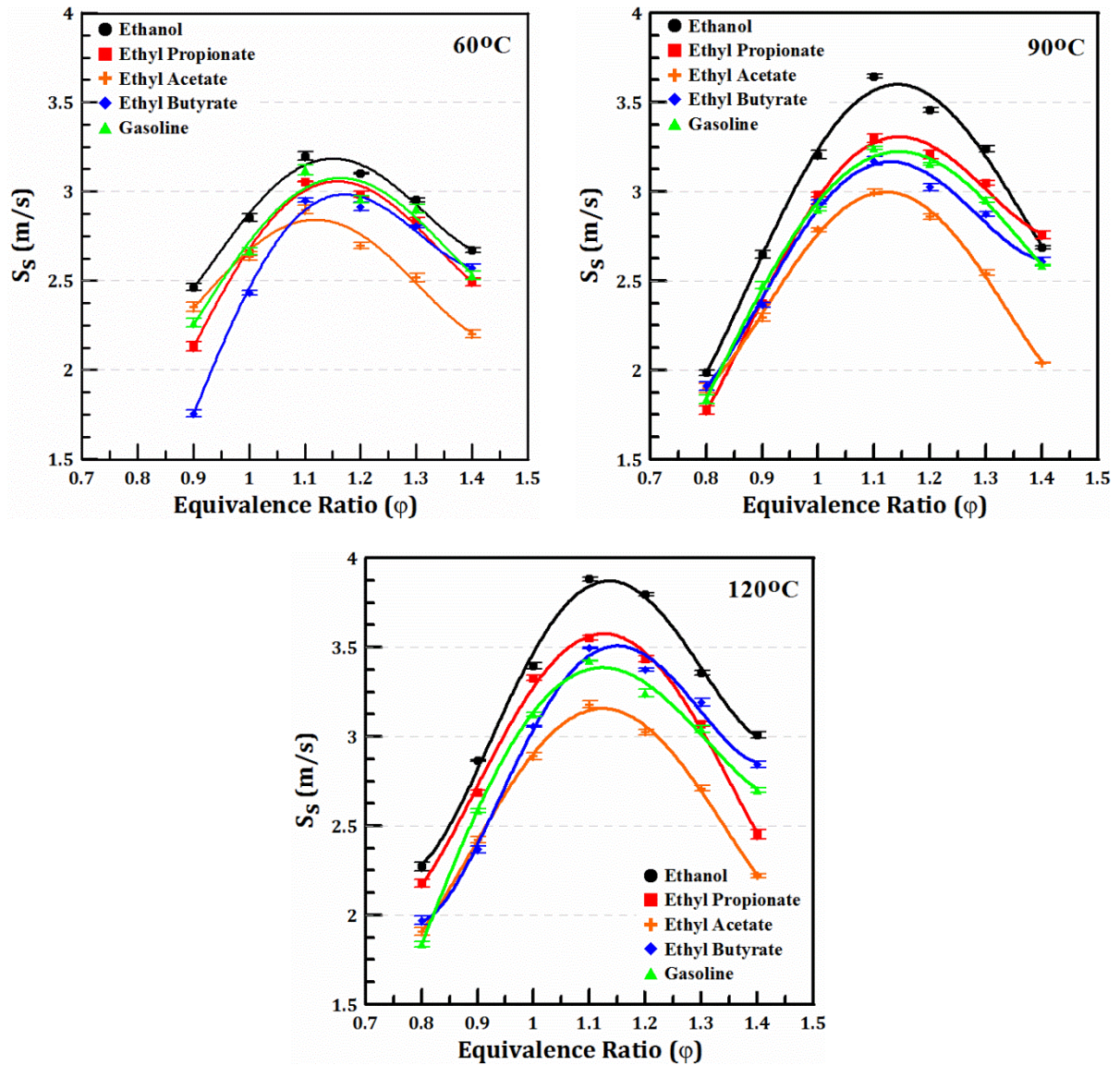
4.3.2. Un-stretched flame propagation speed

The un-stretched flame propagation speeds were obtained by extrapolating the fit line of the stretched flame propagation speeds to a zero stretch rate ($\alpha = 0$), whilst the Markstein lengths were determined by calculating the gradient of the stretched flame propagation speed, utilising the stretch rate slope in the linear range. Figure.6 details the un-stretched flame speeds of the five fuels at different initial temperatures and equivalence ratios. The scattered points indicate the experimental results, whilst the solid lines are quadratic fit curves. The un-stretched flame propagation speed was increased with an increase of the initial temperature due to enhanced chemical reaction rate.

For all examined initial temperatures (60°C, 90°C and 120°C) and equivalence ratios, ethanol had the highest un-stretched flame propagation speeds, whilst EA had the lowest. The highest un-stretched flame speed for ethanol could be due to its molecular structure, which consisted of hydroxyl functional group (-OH) attached to the terminal carbon atoms, leading to a higher un-stretched flame propagation speeds compared to the other fuels [27]. The un-stretched flame speeds of the ethyl ester fuels showed promise when compared with gasoline, especially in the case of EP and EB. At an initial temperature of 60°C, the un-stretched flame speed trend of EP was almost identical to that of gasoline, whilst EB proved lower. However, at high initial temperatures (90°C and 120°C), when compared with gasoline, the trend of EP was greater, whilst EB was faster in rich conditions at 120°C. This is evident at 120°C, where the maximum un-stretched flame propagation speeds of EP and EB were approximately 0.13 m/s and 0.07 m/s respectively, showing an increase relative to gasoline. For the five tested fuels, the peak un-stretched flame speeds occurred in slightly rich mixtures when the equivalence ratio was between 1.0 and 1.2, as expected.

In contrast to EP and EB, as the initial temperature was increased, the difference between the un-stretched flame propagation speeds of EA and gasoline was also increased. It was noticed that at 60°C the maximum un-stretched flame speed of EA was 0.22 m/s slower than gasoline, whilst at 120°C it was 0.25 m/s.

The minimum un-stretched flame propagation speeds for EA compared with EP and EB could be due to dissociation bond energies of C-H. EA had the minimum inner C-H bond compared to EP and EB, therefore EA gives the smallest laminar burning velocity. Also, EA displayed higher sensitivity to the water formation which slower its un-stretched flame speed compared to EP and EB [27, 28].



265 **Figure.6.** Un-stretched flame speed of the test fuels at different temperatures and equivalence ratios (a) 60°C, (b)
 266 90°C and (c) 120°C.
 267

268 **4.3.3. Markstein length, flame thickness and Markstein number**

269

270 The Markstein length indicates the influence of stretch rate on flame propagation speed, which characterizes
 271 the diffusion-thermal instability [15, 29]. Normally, the Markstein length decreases as the equivalence ratio
 272 increases for heavy hydrocarbon–air mixtures, whilst the opposite trend is expected for light hydrocarbon–air
 273 mixtures [30]. **Figure.7** demonstrates the influence of fuel/air equivalence ratio and initial temperature on the
 274 flame/stretch interaction of the five fuels and the burned gases, with the Markstein length (L_b) quantifying the
 275 effect. Generally, the Markstein lengths decreased monotonously with increasing equivalence ratio for each
 276 initial temperature. This was because all the tested fuels were heavy hydrocarbon-air mixtures, and the

277 Markstein length depends on the Lewis number of the fuel for a lean mixture, or that of oxidizer for a rich
278 mixture [30].

279

280

281

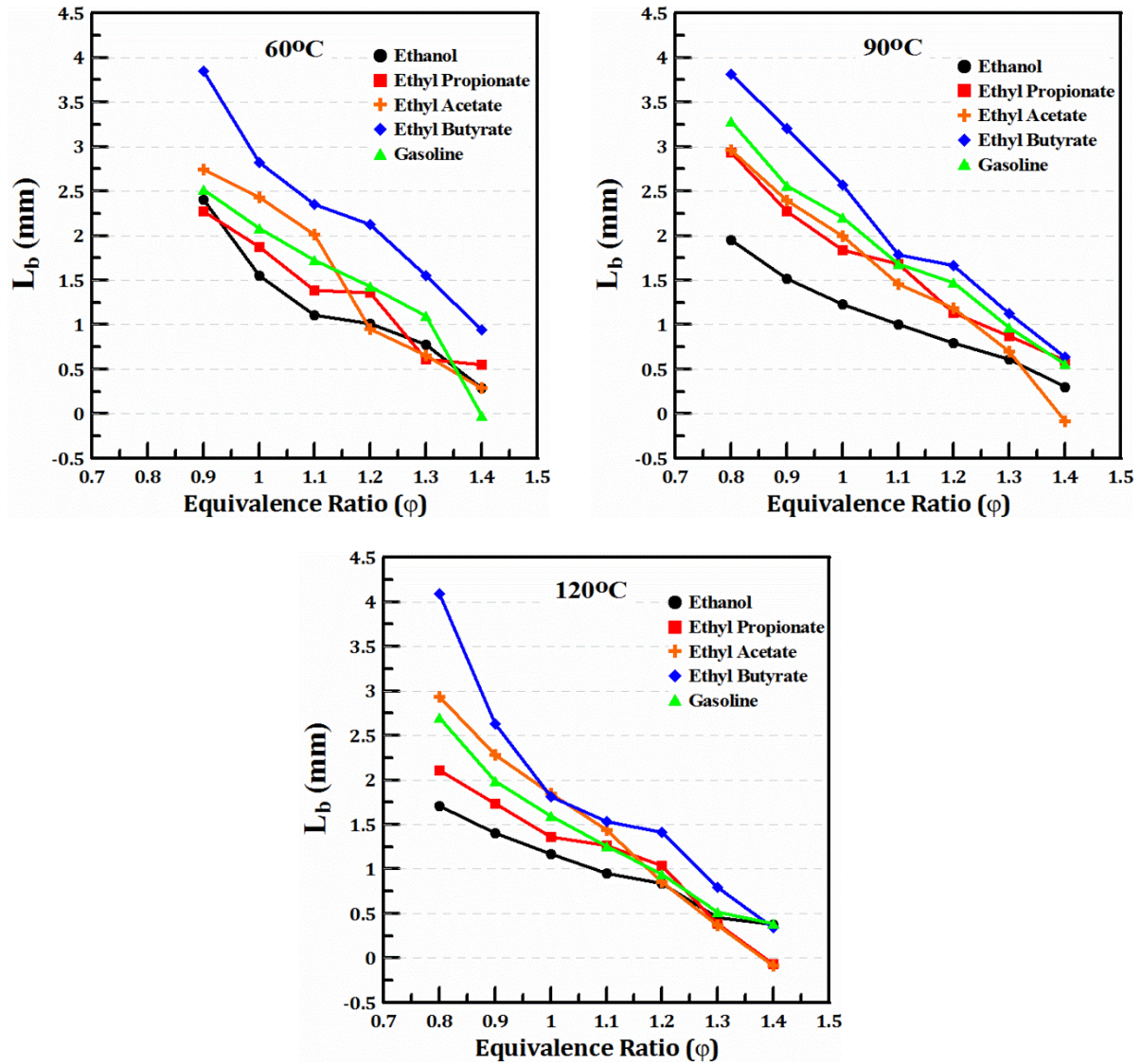
282 For all examined initial temperatures, the Markstein length of EB was the highest among the five fuels, and
283 therefore demonstrated the most stable flame characteristic at the tested condition. EA followed EB in terms of
284 flame stability, exhibiting higher Markstein lengths for $\phi \leq 1.1$, especially at initial temperatures of 60°C and
285 90°C. The Markstein length of ethanol proved to be the smallest among the five fuels, and therefore had the
286 most unstable flame characteristic at the tested condition. Positive Markstein lengths suggested that the flame
287 speed decreases with an increase in the stretch rate, whilst negative Markstein lengths indicated that the flame
288 speed increases with an increase in the stretch rate. Each of the fuels had lower flame speeds when the stretch
289 rate was increased, except EA at $\phi=1.4$, with the negative values of the Markstein length concluding that the EA
290 flame was more unstable at the examined temperatures under rich conditions. Bradley et al. [17] postulated that
291 if the Markstein length is larger than 1.5, the flame will be initially stable until a critical flame radius is reached.
292 This means that EB and EA demonstrate better initial flame stabilities than EP in a lean burning condition.
293 Among the five fuels, EP and ethanol had the weakest initial flame stabilities at different initial temperatures.

293

294 With regards to temperature, the Markstein lengths exhibited higher values at low equivalence ratios ($\phi =$
295 0.8-0.9) when the initial temperature was 60°C, and decreased as the initial temperature was increased. This
296 suggests that rich mixtures and/or high initial temperature lead to instability of the flame front, as the
297 diffusively-thermal stability of lean ethanol-air mixtures was stronger than that of rich mixtures. With respect to
298 the initial temperature, the Markstein length of EB at the lean mixture of $\phi=0.9$ decreased as the temperature
299 increased, with a 31.6% reduction from 3.8mm to 2.6mm. For stoichiometric and rich conditions, the difference
300 in Markstein length of EB was small as the initial temperature increased. The Markstein length for EA
301 decreased as the temperature increased for almost all equivalence ratios, and proved less sensitive to the change
302 of the initial temperature.

303

304



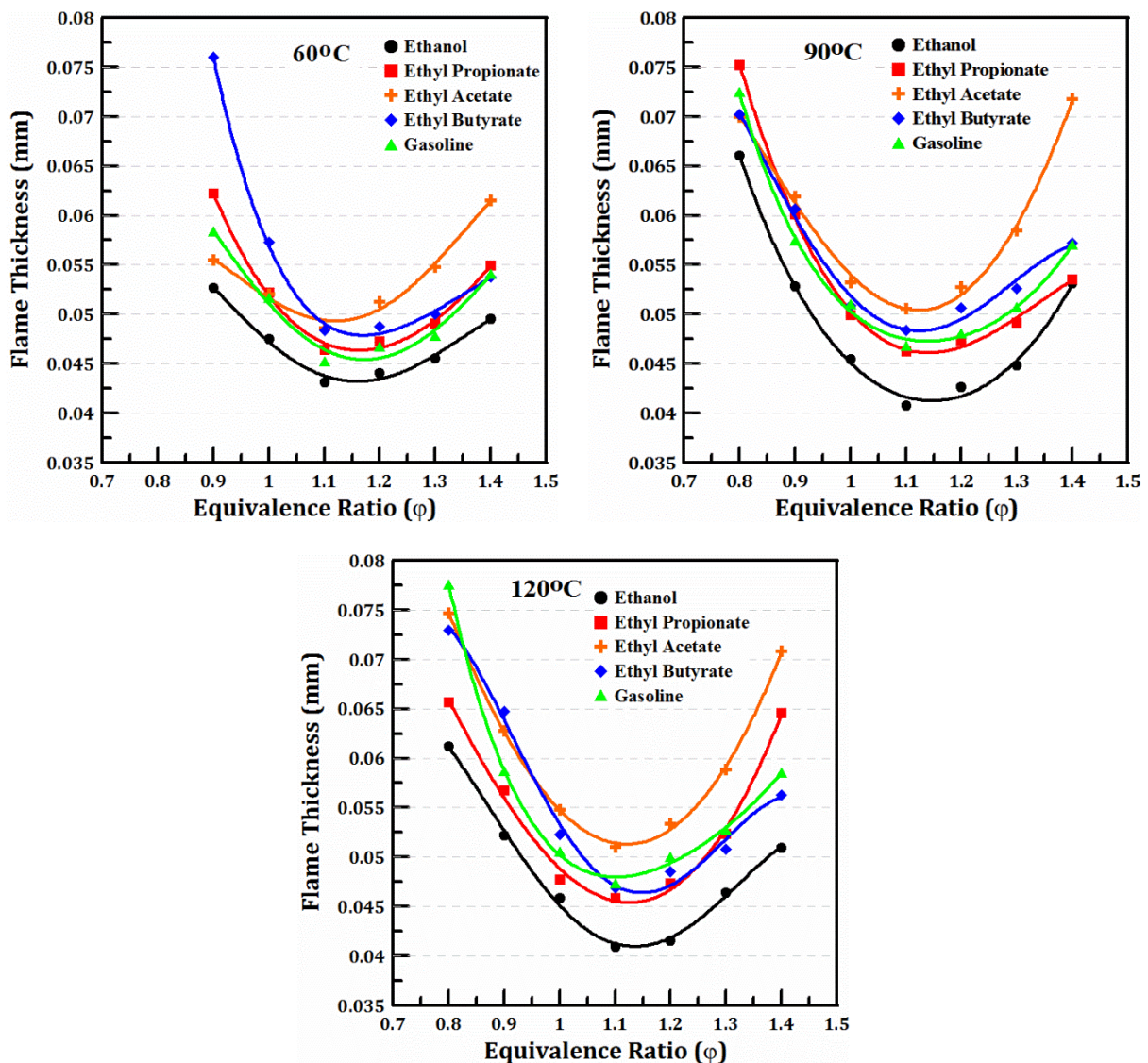
305 **Figure.7.** Markstein length of test fuels at different temperatures and equivalence ratios (a) 60°C, (b) 90°C and (c)
 306 120°C.
 307

308 Two kinds of flame surface instabilities acted on the flame front: the diffusion-thermal instability and the
 309 hydrodynamic instability [15, 31]. The Markstein length was used to characterize the diffusion-thermal
 310 instability, whilst the hydrodynamic instability was determined by the density transition across the flame front,
 311 being represented by the flame thickness and the density ratio. Flame thickness had an inhibiting effect on
 312 hydrodynamic instability, i.e. as the flame thickness decreased, the flame surface instability increased.

313

314 **Figure.8** shows the flame thickness versus equivalence ratio for each of the tested fuels at different initial
 315 temperatures. In general, all the five fuels demonstrated similar trends, with the minimum values occurring near
 316 $\phi=1.1$, indicating higher instability. For all examined initial temperatures, EA yielded the largest flame thickness
 317 among the five fuels at almost all the equivalence ratios, and therefore the lowest hydrodynamic instability. In

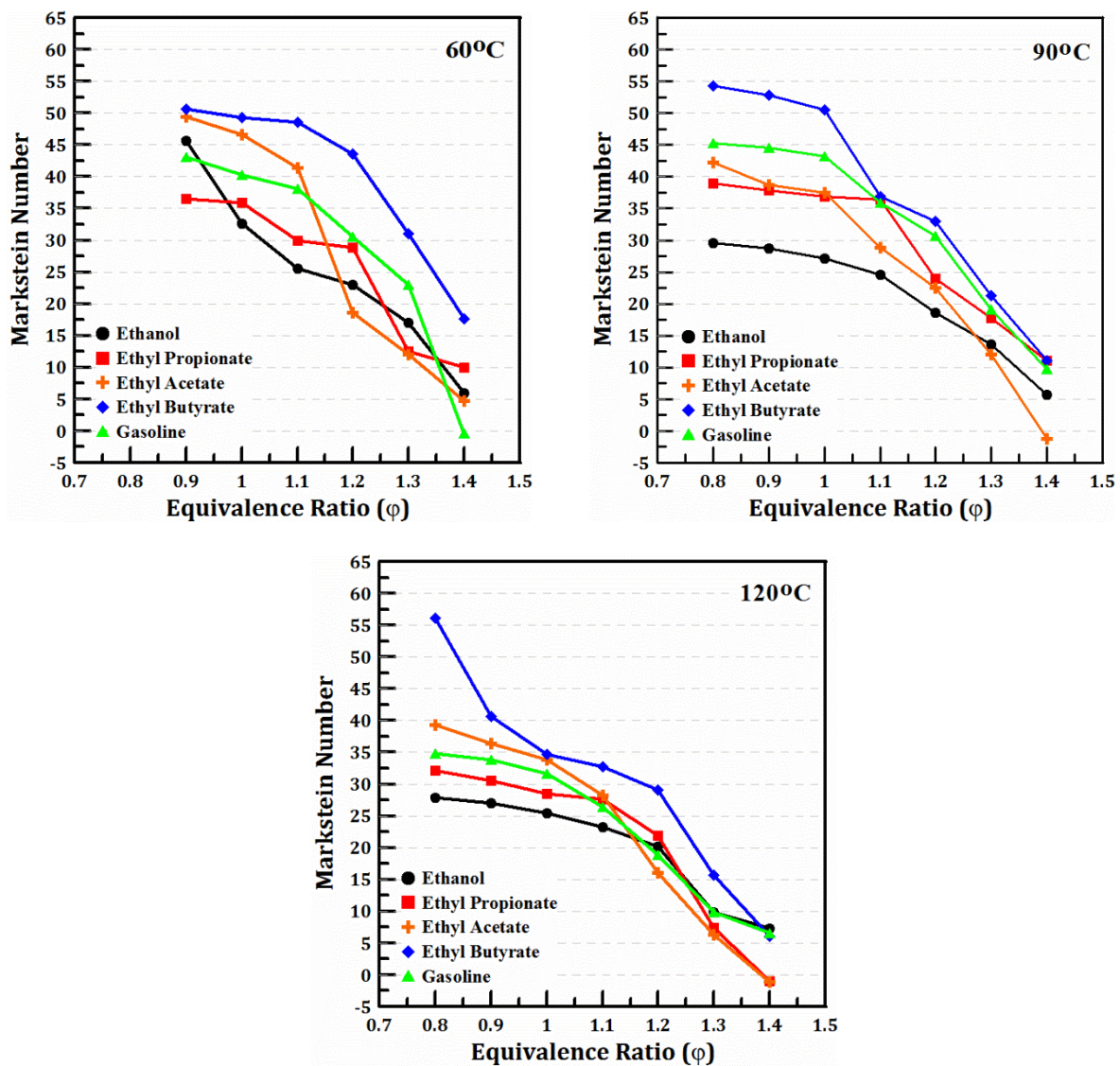
318 contrast to EA, ethanol had the lowest flame thickness and consequently the highest hydrodynamic instability. A
 319 thinner flame usually indicates intensified combustion and faster flame speed, but it also results in lower
 320 tolerance to both internal and external disturbances, making the flame more vulnerable to destabilization. The
 321 results of EP, EB and gasoline proved comparable with each other across all equivalence ratios, and existed
 322 between the trends of EA and ethanol. For each of the five fuels, the flame thickness data was not sensitive to
 323 the variation of initial temperature, except for points around the limits of the lean and rich condition. This
 324 indicated that the initial temperature was not the most important parameter to affect the flame thickness, and
 325 thus the Markstein numbers were determined from the Markstein lengths for the same fuels.



326 Figure.8. Flame thickness of the test fuels at different temperatures and equivalence ratios (a) 60°C, (b) 90°C
 327 and (c) 120°C.

328

329 The effect of local heat release on the flame morphology and the flame front curvature was determined by
 330 the Markstein number, which quantified the response of a laminar flame to stretch and could be used to indicate
 331 the stability of laminar and turbulent flame fronts. Figure.9 details the results of the Markstein number at
 332 different initial temperatures. Lean mixtures yielded high positive values, which decreased as the mixture
 333 became richer, proving similar to the result of the Markstein length. It was observed that the Markstein number
 334 of EB was the highest among the five fuels at the majority of the tested equivalence ratios. Ethanol followed by
 335 EP had the lowest Markstein numbers, which would increase the propensity of the flames to become less stable.



336 Figure.9. Markstein number of the test fuels at different temperatures and equivalence ratios (a) 60°C, (b) 90°C
 337 and (c) 120°C.

338

339

340

341 **4.4. Laminar burning velocities and burning flux**

342

343 The laminar burning velocity was considered a strong function of the equivalence ratio and initial
344 temperature of the reactants [32]. It was defined as the speed at which the flame front was moving towards the
345 unburned mixture. Figure.10 shows the laminar burning velocities versus the equivalence ratios at different
346 initial temperatures. The laminar burning velocities of the five fuels under varying initial temperatures exhibited
347 peaks near the equivalence ratio of 1.1, which correlated to the state of the un-stretched flame speeds.
348 Observation of the five fuels across all examined initial temperatures showed ethanol to yield the highest
349 burning velocity, whilst ethyl acetate had the lowest. Furthermore, it was evident that the laminar flame speeds
350 of the ethyl ester fuels in order of decreasing value were: ethyl propionate (EP) > ethyl butyrate (EB) > ethyl
351 acetate (EA), in general for almost all tested equivalence ratios.

352

353 For the three ethyl esters examined, the experimental data indicated that the burning velocity increased
354 between $\phi = 0.8$ and 1.1, at which a maximum value was observed at different initial temperatures, before
355 decreasing at higher equivalence ratios. Moreover, at an initial temperature of 60°C the maximum burning
356 velocity between the ethyl ester fuels proved similar (at 0.1 MPa bar, 41.2 cm/s for EP, 39.6 cm/s for EB and
357 39.4 cm/s for EA). However, at higher initial temperatures (specifically 120°C), the maximum remained close
358 between EP (55.7 cm/s) and EB (54.52 cm/s), but not when compared with EA (50.1 cm/s).

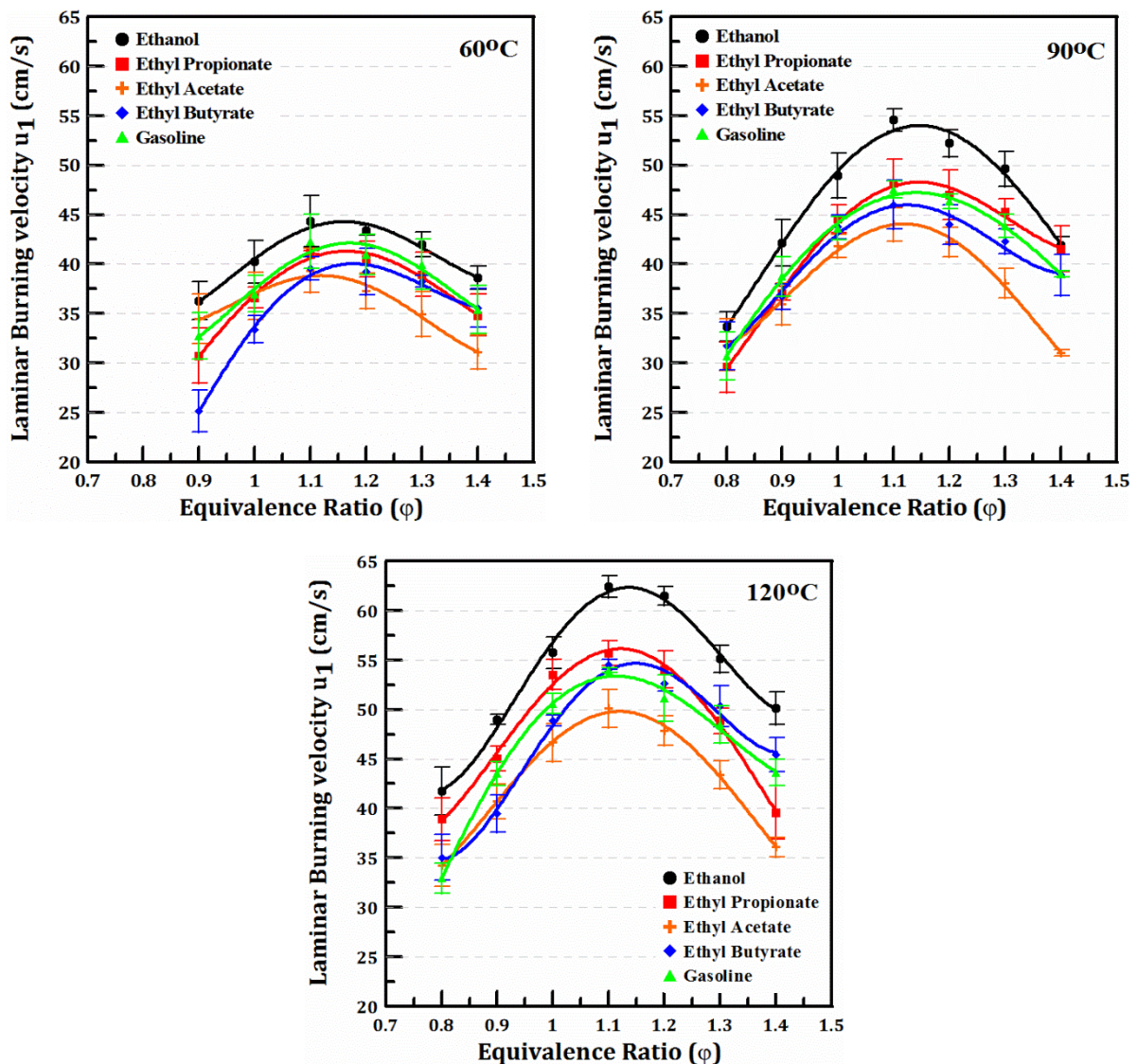
359

360 In comparison with gasoline, the laminar burning velocity of the three ethyl esters showed a competitive
361 velocity profile, especially in the case of EP and EB. For the initial temperature of 60°C, gasoline was more
362 closely matched by EP, although the laminar burning velocity of EP was marginally lower. The maximum
363 burning velocity for gasoline was 42.3 cm/s, whilst for EP it was 41.2 cm/s (a decrease of 2.6%). As the initial
364 temperature was increased to 90°C, the laminar flame speed of EP was matched with that of gasoline, except for
365 rich conditions, with EP proving slightly higher. Further increase of the initial temperature to 120°C resulted in
366 the burning velocity profile of EP to be greater than gasoline. The maximum burning velocity for EP was 55.7
367 cm/s, whilst for gasoline it was 54 cm/s (an increase of 3.2%). For the EB burning velocity, it was noted that as
368 the initial temperature increased, the laminar velocity profile became closer to that of gasoline, especially at
369 120°C where the EB laminar velocity profile proved higher compared to gasoline, especially for rich conditions.
370 The maximum burning velocity for EB was 54.52 cm/s, whilst for gasoline it was 54 cm/s (an increase of 1.0%).

371 In contrast to EP and EB, the peak laminar flame speed of EA decreased as the initial temperature increased
 372 when compared to gasoline. At 60°C the difference in the peak laminar flame speed between gasoline and EA
 373 was 2.9cm/s, whilst at 120°C it was 3.845cm/s.

374

375 The laminar burning velocity proved to have good relation to the equivalence ratio and initial temperature of
 376 the reactants, as expected by theory [33–35]. Figure.10 shows that the laminar burning velocities for all the fuels
 377 increased as the initial temperature increased. For EP, EB and EA, the laminar burning velocities near the peaks
 378 at 120°C were approximately 6–8.5 cm/s faster than the results at 90°C, and approximately 4.6 –7 cm/s faster
 379 than the results at 60°C. At higher equivalence ratios, the difference between burning velocity for EP and EB
 380 were smaller at all examined initial temperatures, and their laminar burning velocities were similar to gasoline.



381 Figure.10. Laminar burning velocities of test fuels at different temperatures and equivalence ratios
 382

383 In order to explain the results, the influence of molecular structure on the different laminar burning velocities
384 was discussed. The highest laminar flame speed for ethanol could be due to its molecular structure, which
385 consisted of hydroxyl functional group (-OH) attached to the terminal carbon atoms, leading to a higher laminar
386 burning velocity compared to the other fuels [27, 36]. In the aspect of chemical kinetics, bond energy was used
387 to investigate the flame speed difference among the ester fuel isomers. Gu et al. [27] demonstrated that isomers
388 with more methyl groups have lower laminar flame speeds due to the high energy of the C-H bond in the
389 methyl group. Ethanol had only one methyl group compared the ethyl ester fuels isomers which consists of two
390 methyl group, thus leading to higher laminar flame speed for ethanol compared to ester fuels. The influence of
391 the methyl group on the laminar flame speed for the ethyl ester fuels was eliminated due to their similar methyl
392 group configuration.

393

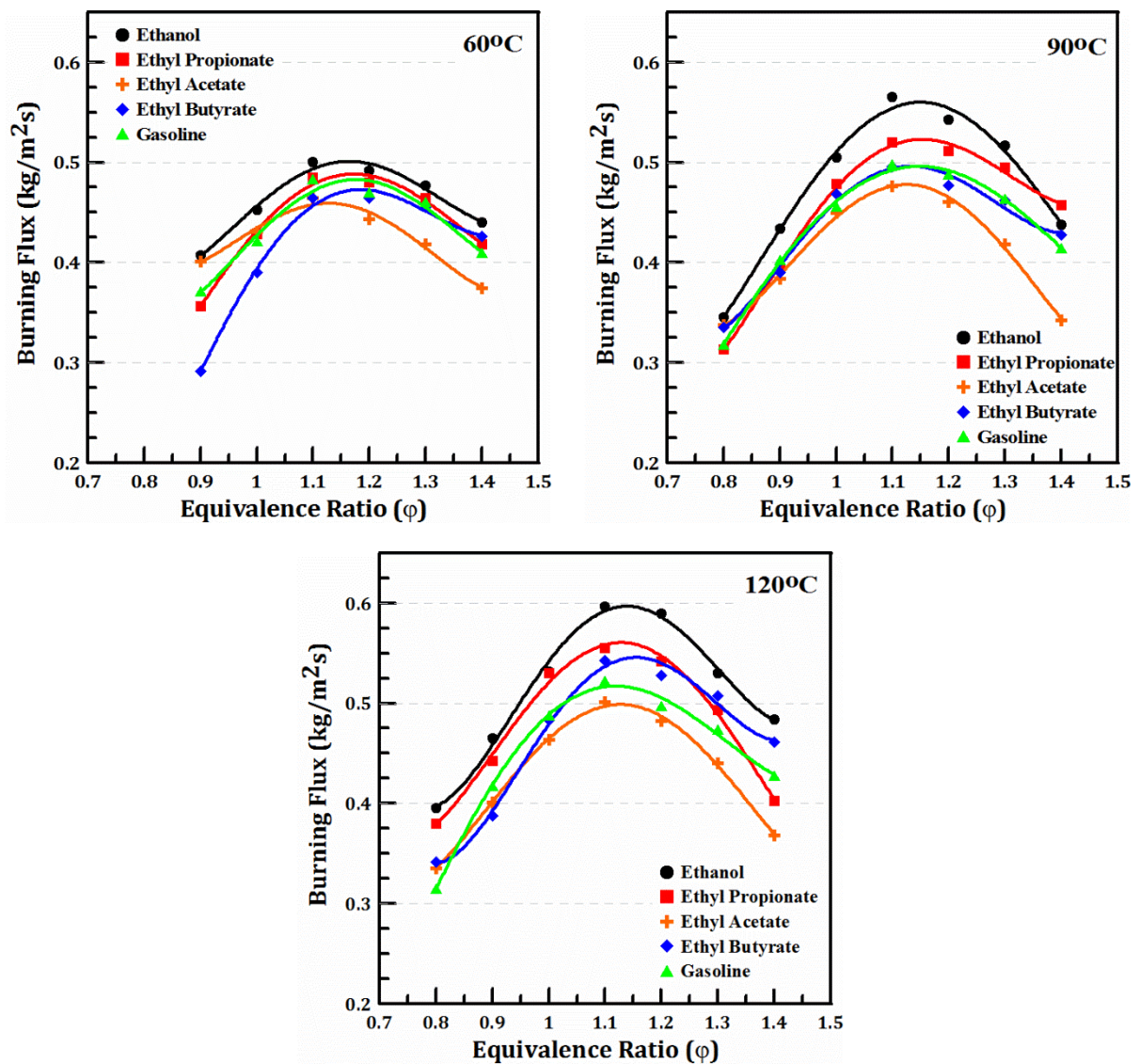
394 Furthermore, dissociation bond energies of C-H on the terminal carbon atoms (terminal C-H) were larger
395 than those of C-H on the inner carbon atoms (inner C-H) [27]. H atom was easily abstracted from the inner
396 carbon atoms compared to that from the terminal carbon atoms. EP and EB had most inner C-H bonds compared
397 to EA. Weak inner C-H bond energies in EP and EB facilitated the H-abstraction reaction compared to EA
398 isomers, which had less inner C-H bonds. With more inner C-H bonds, EP and EB yielded the largest laminar
399 burning velocity, whilst EA with minimum inner C-H bond displayed the smallest laminar burning velocity. The
400 phenomenon of C-H bonds qualitatively agrees with the variation of laminar burning velocity, and this
401 suggested that laminar burning velocities of ester isomers-air mixtures strongly depend on the bond dissociation
402 energies.

403

404 Dayma et al. [28] investigated the sensitivity analyses of EP, EB and EA on the laminar flame speed at 0.1
405 MPa, 423 K, and equivalence ratios of 0.7, 1.0, and 1.4. They revealed that the most sensitive reaction,
406 regardless of the equivalence ratio and the ester, was the branching reaction, $H + O_2 \rightleftharpoons OH + O$, which
407 accelerated the flame. The sensitivity of this reaction increased with the equivalence ratio, and EA demonstrated
408 slightly higher sensitivity compared to EP and EB. Moreover, they displayed that water formation by
409 recombination of H and OH slowed the flame with a sensitivity slightly increasing with the equivalence ratio.
410 EA demonstrated higher sensitivity to the water formation which slowed its laminar flame speed compared to
411 EP and EB. The minimum sensitivity for the water formation was noticed for EP.

412

413 Figure.11 shows the burning flux versus equivalence ratio for the five fuels at different initial temperatures.
 414 The laminar burning flux reveals the eigenvalue of the flame propagation, which was obtained by multiplying
 415 the laminar burning velocity with the density of the unburned mixture. The general trend was similar to that of
 416 laminar burning velocity, where laminar burning velocity was the main influencing factor. However, the larger
 417 density of the EP-air mixture in comparison to the gasoline-air mixture contributed to a larger burning flux at all
 418 examined initial temperatures. At 90°C, EB demonstrated a similar trend to gasoline, whilst at 120°C it proved
 419 higher for $\Phi > 1.1$. Among the five fuels, ethanol yielded the highest laminar burning flux, whilst EA had the
 420 lowest. The peak values of all the fuels at the three temperatures existed between equivalence ratios of 1.0 and
 421 1.2. Furthermore, with respect to temperature, the laminar burning flux of all the fuels increased as the initial
 422 temperature increased.



423 Figure.11. Burning flux of test fuels at different temperatures and equivalence ratios (a) 60°C, (b) 90°C and (c)
 424 120°C

425 **Conclusions**

426 Laminar combustion characteristics of ethanol, gasoline, EP, EB and EA–air mixtures were investigated
427 using high-speed schlieren photography at initial temperatures of (60°C, 90°C and 120°C) over wide range of
428 equivalence ratios ($\phi = 0.8-1.4$) under 0.1 MPa initial pressure in a constant volume vessel. The characteristics
429 of the ethyl ester fuels were compared to the cases of ethanol and gasoline. The main conclusions are
430 summarized as follows:

431

432 1. The un-stretched flame speeds of EP, EB and EA were lower than that of ethanol and gasoline at an initial
433 temperature of 60°C. As the initial temperature increased to 90°C and 120°C, the un-stretched flame speeds of
434 EP also increased, relative to gasoline. At 120°C, the un-stretched flame speeds of EB increased compared to
435 gasoline, especially for rich conditions. EA consistently displayed the lowest un-stretched flame speeds among
436 the five fuels.

437

438 2. The EB and EA flames proved more stable compared to ethanol and gasoline at equivalence ratios lower
439 than 1.1 for 60°C and 120°C. EP demonstrated greater flame stability than ethanol, however less when compared
440 to gasoline at equivalence ratios lower than 1.0, at all examined temperatures. The flame thickness results
441 showed that EB and EA presented a lower hydrodynamic instability performance among the five fuels for most
442 of the test points. The Markstein numbers displayed similar trends as the Markstein lengths for the current tests.

443

444 3. The laminar burning velocities of the EP fuels proved faster compared to EB and EA, whilst slower
445 compared to ethanol and gasoline at 60°C. As the initial temperature increased, up to 120°C, the laminar flame
446 speed of EP and EB became faster, when compared to gasoline. The lowest laminar burning velocity was
447 observed for EA among all the five fuels. Moreover, at an initial temperature of 60°C the maximum burning
448 velocity between the ethyl ester fuels proved similar (at 0.1 MPa, 41.2 cm/s for EP, 39.6 cm/s for EB and 39.4
449 cm/s for EA). However, at higher initial temperatures (120°C), the maximum burning velocity remained close
450 between EP (55.7 cm/s) and EB (54.52 cm/s), but not when compared to that of EA (50.1 cm/s).

451

452 The results of this investigation showed that ethyl ester fuels demonstrated robust combustion characteristics,
453 especially EP and EB, when compared to ethanol and gasoline. For future work, a detailed study of the effect of

454 ethyl ester fuels on the engine performance and emissions in Gasoline Direct Injection (GDI) engine would
455 ensure an enhanced consideration of the advantages of ethyl ester fuels as surrogate fuels for gasoline.

456 **References**

- 457 [1] Köpke M, Noack S and Dürre P. The Past, The Present, and Future of Biofuels – Biobutanol as Promising
458 Alternative. In: dos Santos Bernardes MA (ed.) Biofuel Production – Recent Developments and Prospects.
459 Rijeka, Croatia: InTech, 2011, pp.451–486. DOI: [10.5772/20113](https://doi.org/10.5772/20113)
- 460 [2] Harnisch F, Nilges P, Blei I et al. From the test-tube to the test-engine: assessing the suitability of
461 prospective liquid biofuel compounds. RSC Advances 2013; 3: 9594–9605. DOI: [10.1039/C3RA40354H](https://doi.org/10.1039/C3RA40354H)
- 462 [3] Nuffield Council on Bioethics. Biofuels: ethical issues. Report, Nuffield Press, UK, April 2011.
- 463 [4] Carels N. The Challenges of Bioenergies: An Overview. In: dos Santos Bernardes MA (ed.) Biofuel's
464 Engineering Process Technology. Rijeka, Croatia: InTech, 2011, pp.23–64. DOI: [10.5772/16403](https://doi.org/10.5772/16403)
- 465 [5] Tian G, Daniel R, Li H, Xu H, Shuai S, Richards P. Laminar burning velocities of 2,5-dimethylfuran
466 compared with ethanol and gasoline. Energy & Fuels. 2010; 24:3898-3905. DOI: [10.1021/ef100452c](https://doi.org/10.1021/ef100452c)
- 467 [6] Román-Leshkov Y, Barrett CJ, Zhen YL et al. Production of dimethylfuran for liquid fuels from biomass-
468 derived carbohydrates. Nature and Science 2007; 447: 982–985. DOI:[10.1038/nature05923](https://doi.org/10.1038/nature05923)
- 469 [7] Ma X, Jiang C, Xu H et al. Laminar burning characteristics of 2-methylfuran compared with 2, 5-
470 dimethylfuran and isooctane. Energy & Fuels 2013; 27(10): 6212–6221. DOI: [10.1021/ef401181g](https://doi.org/10.1021/ef401181g)
- 471 [8] Tian G, Daniel R and Xu H. DMF – A New Biofuel Candidate. In: dos Santos Bernardes MA (ed.) Biofuel
472 Production – Recent Developments and Prospects. Rijeka, Croatia: InTech, 2011, pp.487–520. DOI:
473 [10.5772/21738](https://doi.org/10.5772/21738)
- 474 [9] Contino F, Foucher F, Mounaïm-Rousselle C et al. Engine performances and emissions of second-
475 generation biofuels in spark ignition engines: the case of methyl and ethyl valerates. SAE paper 2013-24-
476 0098, 2013. DOI:[10.4271/2013-24-0098](https://doi.org/10.4271/2013-24-0098)
- 477 [10] Jenkins RW, Munro M, Nash S et al. Potential renewable oxygenated biofuels for the aviation and road
478 transport sectors. Fuel 2013; 103: 593–599. DOI: [10.1016/j.fuel.2012.08.019](https://doi.org/10.1016/j.fuel.2012.08.019)
- 479 [11] Contino F, Foucher F, Mounaïm-Rousselle C et al. Experimental Characterisation of Ethyl Acetate, Ethyl
480 Propionate, and Ethyl Butanoate in a Homogeneous Charge Compression Ignition Engine. Energy & Fuels
481 2011; 25 (3): 998–1003. DOI:[10.1021/ef101602q](https://doi.org/10.1021/ef101602q)

- 482 [12] Contino F, Foucher F, Mounaïm-Rousselle C et al. Combustion Characteristics of Tricomponent Fuel
483 Blends of Ethyl Acetate, Ethyl Propionate, and Ethyl Butyrate in Homogeneous Charge Compression
484 Ignition (HCCI). *Energy & Fuels* 2011; 25 (4): 1497–1503. DOI: [10.1021/ef200193q](https://doi.org/10.1021/ef200193q)
- 485 [13] Olson ES, Aulich TR, Sharma RK, Timpe RC. Ester fuels and chemicals from biomass. *Biotechnology for*
486 *Fuels and Chemicals*: Springer; 2003. p. 843-851. DOI: [10.1385/ABAB:108:1-3:843](https://doi.org/10.1385/ABAB:108:1-3:843)
- 487 [14] Dabbagh H, Ghobadi F, Ehsani M, Moradmand M. The influence of ester additives on the properties of
488 gasoline. *Fuel*. 2013; 104:216-223. DOI: [10.1016/j.fuel.2012.09.056](https://doi.org/10.1016/j.fuel.2012.09.056)
- 489 [15] Law CK, Sung CJ. Structure, aerodynamics, and geometry of premixed flamelets. *Prog Energy Combust*
490 *Sci* 2000;26:459–505. DOI.org/10.1016/S0360-1285(00)00018-6
- 491 [16] Beeckmann J, Röhl O, Peters N. Experimental and numerical investigation of iso-octane, methanol and
492 ethanol regarding laminar burning velocity at elevated pressure and temperature. SAE Technical Paper
493 2009-01-1774; 2009. DOI:10.4271/2009-01-1774
- 494 [17] Bradley D, Hicks RA, Lawes M, Sheppard CGW, et al. The measurement of laminar burning velocities and
495 Markstein numbers for iso-octane-air and isooctane- n-heptane-air mixtures at elevated temperatures and
496 pressures in an explosion bomb. *Combust Flame* 1998; 115:126–144.
- 497 [18] Gu XJ, Haq MZ, Lawes M, Woolley R. Laminar burning velocity and Markstein lengths of methane–air
498 mixtures. *Combust Flame* 2000; 121:41–58. DOI: [10.1016/S0010-2180\(99\)00142-X](https://doi.org/10.1016/S0010-2180(99)00142-X)
- 499 [19] Turns SR. *An introduction to combustion*. New York: McGraw-Hill; 1996.
- 500 [20] Olikara C, Borman GL. A computer program for calculating properties of equilibrium combustion products
501 with some applications to I.C. engines. SAE Technical Paper 750468; 1975. DOI:10.4271/750468
- 502 [21] Wu X, Huang Z, Wang X, et al. Laminar burning velocities and flame instabilities of 2,5-dimethylfuran–air
503 mixtures at elevated pressures. *Combust Flame* 2011; 158(3): 539–546 DOI:
504 [10.1080/00102202.2010.516037](https://doi.org/10.1080/00102202.2010.516037)
- 505 [22] Wu X, Li Q, Fu J, et al. Laminar burning characteristics of 2,5-dimethylfuran and iso-octane blend at
506 elevated temperatures and pressures. *Fuel* 2012; 95:234–240. doi:10.1016/j.fuel.2011.11.057
- 507 [23] Bradley D, Lawes M, Mansour M. Explosion bomb measurements of ethanol–air laminar gaseous flame
508 characteristics at pressures up to 1.4 MPa. *Combustion and Flame*. 2009; 156:1462-1470. DOI:
509 [10.1016/J.COMBUSTFLAME.2009.02.007](https://doi.org/10.1016/J.COMBUSTFLAME.2009.02.007)

- 510 [24] Liao S, Jiang D, Huang Z, Zeng K, Cheng Q. Determination of the laminar burning velocities for mixtures
511 of ethanol and air at elevated temperatures. *Applied Thermal Engineering*. 2007;27: 374-380. DOI:
512 [10.1016/j.applthermaleng.2006.07.026](https://doi.org/10.1016/j.applthermaleng.2006.07.026)
- 513 [25] Burke MP, Chen Z, Ju Y, Dryer FL. Effect of cylindrical confinement on the determination of laminar
514 flame speeds using outwardly propagating flames. *Combust Flame* 2009; 156:771–779. DOI:
515 [10.1016/J.COMBUSTFLAME.2009.01.013](https://doi.org/10.1016/J.COMBUSTFLAME.2009.01.013)
- 516 [26] Li Q, Tang C, Cheng Y, Guan L, Huang Z. Laminar Flame Speeds and Kinetic Modeling of n-Pentanol and
517 Its Isomers. *Energy & fuels*. 2015; 29: 5334-5348. DOI: [10.1021/acs.energyfuels.5b00740](https://doi.org/10.1021/acs.energyfuels.5b00740).
- 518 [27] Gu X, Huang Z, Wu S, Li Q. Laminar burning velocities and flame instabilities of butanol isomers–air
519 mixtures. *Combustion and Flame*. 2010; 157:2318-2325. DOI: [10.1016/j.combustflame.2010.07.003](https://doi.org/10.1016/j.combustflame.2010.07.003)
- 520 [28] Dayma G, Halter F, Foucher F, Mounaim-Rousselle C, Dagaut P. Laminar burning velocities of C4–C7
521 ethyl esters in a spherical combustion chamber: Experimental and detailed kinetic modeling. *Energy*
522 & *Fuels*. 2012 Oct 10; 26(11):6669-6677. DOI: [10.1021/ef301254q](https://doi.org/10.1021/ef301254q)
- 523 [29] Karlin V, Sivashinsky G. Asymptotic modelling of self-acceleration of spherical flames. *Proc Combust*
524 *Inst* 2007; 31:1023–1030. DOI: [10.1016/j.proci.2006.07.233](https://doi.org/10.1016/j.proci.2006.07.233)
- 525 [30] Bechtold JK, Matalon M. The dependence of the Markstein length on stoichiometry. *Combust Flame*
526 2001; 127:1906–1913. DOI: [10.1016/S0010-2180\(01\)00297-8](https://doi.org/10.1016/S0010-2180(01)00297-8)
- 527 [31] Matalon M. Intrinsic flame instabilities in premixed and non-premixed combustion. *Annu Rev Fluid*
528 *Mech* 2007; 39:163–191. DOI: [10.1146/annurev.fluid.38.050304.092153](https://doi.org/10.1146/annurev.fluid.38.050304.092153)
- 529 [32] Stone, R. Introduction to internal combustion engine, laminar burning velocity, 3rd Edition. London. 1999;
530 pp 363-365.
- 531 [33] Stone Richard. Introduction to internal combustion engine. SAE International and Macmillan Press; 2012.
- 532 [34] Hirasawa T, Sung CJ, Joshi A, Yang Z, Wang H, Law CK. Determination of laminar flame speeds using
533 digital particle image velocimetry: binary fuel blends of ethylene, n-Butane, and toluene. *Proc Combust*
534 *Inst* 2002; 29:1427–1434. DOI: [10.1016/S1540-7489\(02\)80175-4](https://doi.org/10.1016/S1540-7489(02)80175-4).
- 535 [35] Tang CL, Huang ZH, Law CK. Determination, correlation, and mechanistic interpretation of effects of
536 hydrogen addition on laminar flame speeds of hydrocarbon–air mixtures. *Proc Combust Inst* 2011;
537 33:921–928. DOI: [10.1016/j.proci.2010.05.039](https://doi.org/10.1016/j.proci.2010.05.039).

538 [36] Gong J, Zhang S, Cheng Y, Huang Z, Tang C, Zhang J. A comparative study of n-propanol, propanal,
 539 acetone, and propane combustion in laminar flames. Proceedings of the Combustion Institute. 2015 Dec
 540 31; 35(1):795-801. DOI: 10.1016/j.proci.2014.05.066.

541
 542
 543

Paper Abbreviations

RON	Research Octane Number	EA	Ethyl acetate
EP	Ethyl propionate	EB	Ethyl butyrate
2MF	2-methylfuran	2,5DMF	2, 5-dimethylfuran
DFB	dual fermentation bio-refinery	SI	Spark ignition
CI	Compression ignition	HCCI	Homogeneous charge compression ignition
PRF95	Primary Reference Fuels	S_n	Stretched laminar flame speed
r_u	Instantaneous flame radius	α	Stretch rate
L_b	Markstein length	S_s	Unstretched laminar flame speed
ρ_b	Burned mixture densities	ρ_u	Unburned mixture densities
n_u	Number of reactant moles	n_b	Number of product moles
T_u	Initial temperature	T_b	Adiabatic flame temperature
ν	kinematic viscosity	u_l	Laminar burning velocity
LHV	Lower heating value	δ_L	flame thickness
Ma	Markstein number	f	laminar burning flux
ϕ	Fuel-air equivalence ratio		

544